Available online at www.sciencedirect.com
SCIENCE DIRECT®
Biosensors and Bioelectronics 18 (2003) 511–519
BIOSENSORS & BIOELECTRONICS
www.elsevier.com/locate/bios

Reagentless detection of microorganisms by intrinsic fluorescence

Cory Estes, Andrew Duncan, Brad Wade, Christopher Lloyd, Walther Ellis, Jr., Linda Powers *

Department of Electrical Engineering, National Center for the Design of Molecular Function, Utah State University, Logan, UT 84322-4155, USA

Received 9 September 2002; received in revised form 23 October 2002; accepted 1 November 2002

Abstract

Quick and accurate detection of microbial contamination is accomplished by a unique combination of leading-edge technologies described in this and the accompanying paper. In this contribution, a hand-held prototype instrument is described which is capable of statistically sampling the environment for microbial contamination and determining cell viability. The technology is sensitive enough to detect very low levels (~ 20 cells/cm^2 or cm^3) of microbes in seconds.

Keywords: Microbe sensor; Intrinsic fluorescence; Optical detection; Microbial contamination

1. Introduction

Recent outbreaks of sickness and deaths from microbial contamination of food highlight the seriousness of this health risk. These emphasize the importance of quick and accurate assessment of microbial contamination. This and the following contribution *Taxonomic identification of microorganisms by capture and intrinsic fluorescence detection* couple leading-edge technologies to detect and identify the nature of microbial contamination of food, water, air, and surfaces.

Many current diagnostic technologies (Hobson et al., 1996; Henchal et al., 2001) require outgrowth/capture of the microbes in the detection protocols. This step requires hours to days, and may fail to detect viable (but non-culturable) cells; instead, the growth medium may favor the growth of bacteria with specific phenotypes. Regardless of the characterization technology, the samples must be taken in the 'right spot' to accurately evaluate the presence and/or distribution of the microbial flora, since it is impossible to sample large areas/volumes or continuously sample with current technology. Sample contact itself is a major concern in most situations.

Fluorescence methods have been shown to provide the most sensitive detection of biomolecules. The high sensitivity, short-collection-time requirement, in situ measurement capability with no sample contact, and the capability of monitoring large areas/volumes continuously render fluorescence methods attractive for the investigation of bacterial cells. Furthermore, the fluorescence intensity is proportional to the excitation intensity, and so even weak signals can be observed by using high-power illumination. One fluorescence-based approach uses the intrinsic fluorescence of tryptophan, other amino acids, and DNA, which are excited and fluoresce in UV (200–300 nm excitation, 300–400 nm emission). Observation of these markers is a sensitive indicator of the presence of biological materials. However, all biological materials contain these fundamental building blocks and, in addition, particles, such as dust, pollen, smoke, etc., preferentially scatter UV/blue radiation (Rayleigh scattering). These interferences significantly reduce the efficacy of using these markers alone to unambiguously detect microbial contamination.

A variety of cell components exhibit intrinsic fluorescence: reduced pyridine nucleotides (RPNs), tryptophan, tyrosine, DNA, lumazines, pterins, flavoproteins, and other secondary metabolites (Nealson and Hastings, 1979; Dalterio et al., 1987; Glazier and Weethall, 1994). Of these, RPN and the amino acids have been the most extensively studied (e.g. Duysens

* Corresponding author. Tel.: +1-435-797-2033; fax: +1-435-797-3328.
E-mail address: lsp@biocat.ece.usu.edu (L. Powers).

0956-5663/03/$ - see front matter
doi:10.1016/S0956-5663(03)00008-3

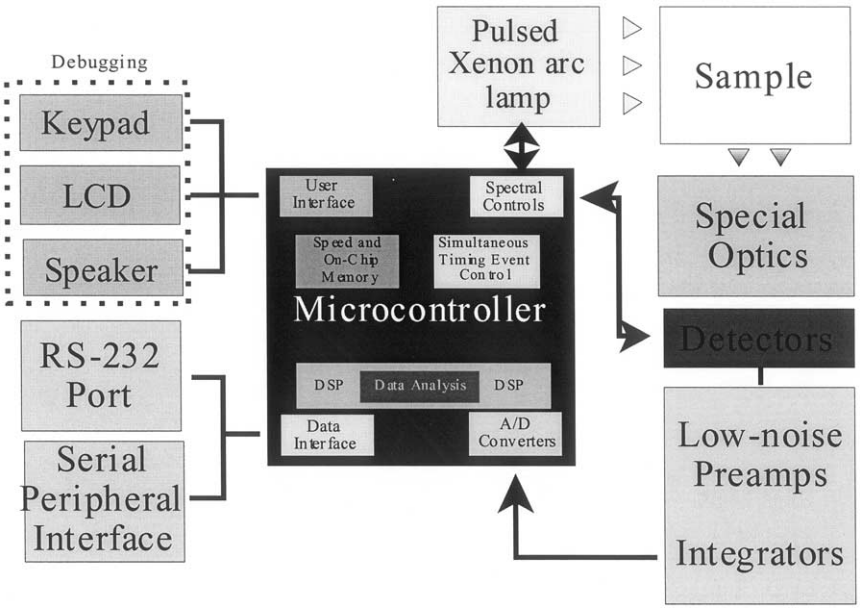

Fig. 1. System block diagram.

and Amesz, 1957; Chance and Theorell, 1959; Galeotti et al., 1970; Barlow and Chance, 1976; Mayevsky and Chance, 1982; Luong and Mulchandani, 1990; Kierdaszuk et al., 1996; see, for a review Lackowicz, 1991) and have excitation energies in the UV region. The metabolic signals can be obtained by integration of the 425–500 nm region fluorescence (340–360 nm excitation). This fluorescence is directly proportional to the concentration of the metabolite, e.g., RPN, which is related to the number of 'live' (metabolizing) cells. Variations within a factor of 10 or so are observed depending on the metabolic state and the microbial species. Other components, such as flavoproteins and cytochromes, have some absorption in this region, but their concentrations are factors of 10–100 less in living cells. Flavoproteins fluoresce in the visible (500–600 nm) with 420–500 nm excitation. In fact, there are no interferences of biological origin in this region and this fact has made redox fluorimetry based on RPN and flavoproteins, a vital tool in the investigation of cellular metabolism and tissue oxygenation (Galeotti et al., 1970; Barlow and Chance, 1976; Mayevsky and Chance, 1982; Luong and Mulchandani, 1990). RPN fluorescence from a single yeast cell was observed in 1959 by Chance and Theorell with an arc lamp and a microscope (5). The Ca^{2+}-dipicolinic acid complex, an integral component of spores (15–30%) but otherwise rare in nature, has characteristic fluorescence in the blue region with UV excitation (Lloyd et al., 2001; Powers and Ellis, 2001; Powers et al., 2002).

We have developed a method and prototype devices for the detection of microbes on surfaces, such as food, glass, plastic, cloth, stainless steel, etc., in air and water/liquids, which have demonstrated a sensitivity of ~ 20 cells/cm^2 or cm^3 under environmental conditions.

2. Experimental

A variety of bacterial cells and yeast were used (see accompanying paper). All cells were grown just past mid-log phase, centrifuged at $3750 \times g$ for 5 min, then washed once with minimal media. The pellet was centrifuged again (same conditions) and re-suspended in minimal media. The concentration was estimated to be 10^7 ml^{-1}. Cells were counted using a Petroff-Hauser cell counting chamber.

A minimal medium was prepared specifically to have no fluorescence background by the following method. In 1 l of deionized water, 0.5 g of NaCl, 1.0 g ammonium sulfate, 10 g Trizma·HCl, 0.3 g $MgSO_4$, 2 g glucose, 5 mg $CaCl_2$, 10 ml of 20% glycerol, and 0.5 g alanine were added. In addition, 5 mg of the following amino acids were added: cysteine, methionine, glycine, glutamic acid, serine, proline, and threonine together with trace amounts of $ZnSO_4$, $FeSO_4$, and $CuSO_4$. The pH of the resulting solution was adjusted to 7.2 and then filter sterilized.

3. Results and discussion

The system block diagram for a prototype instrument is shown in Fig. 1 (Lloyd et al., 2001). Two patents on this technology have recently issued (Powers, 1998, 1999). These prototypes employ multiple intrinsic fluorescence markers of metabolites, which are present only

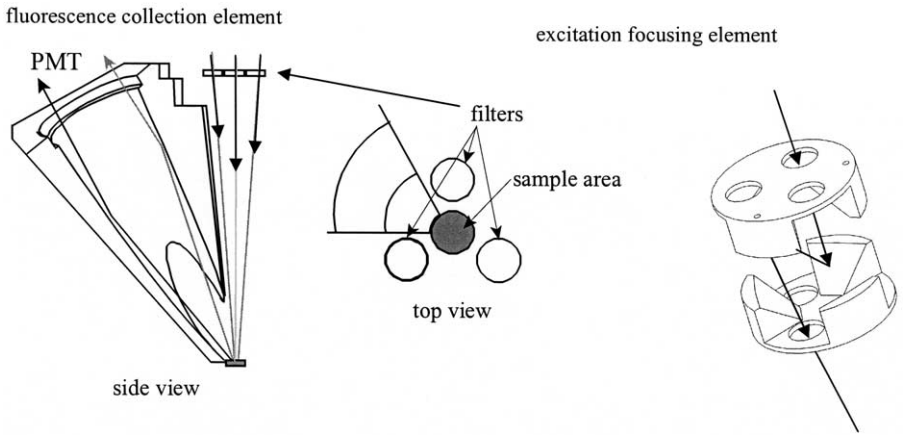

Fig. 2. Excitation and emission optical elements.

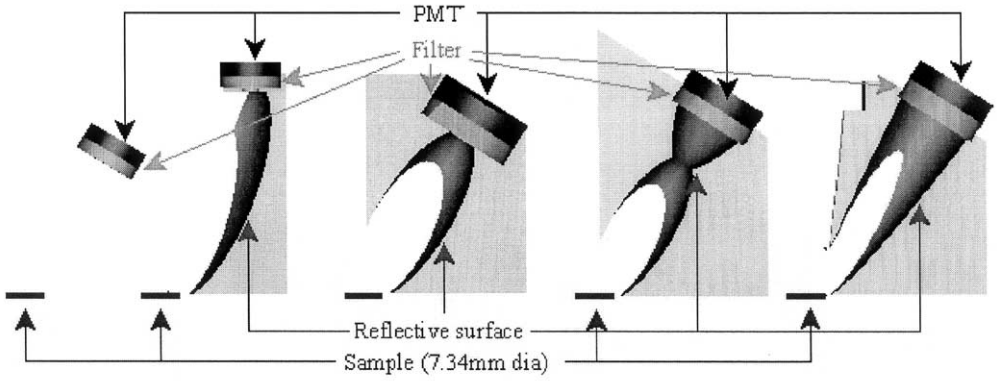

	No Element	Partial Ellipsoid		Ellipsoid		Ellipsoid/paraboloid		Paraboloid	
	PMT		PMT		PMT		PMT		PMT
Bounces	(8mm)	Filter	(8mm)	Filter	(8mm)	Filter	(24.5mm)	Filter	(50mm)
1	20	730	1	951	1	535	1	1007	1
3	0	30	0	198	0	561	121	100	1006
7	0	2	290	1	124	20	496	6	105
>7	0	0	0	0	0	0	0	1	2
Angles									
5	20	53	50	39	39	335	335	646	646
10	0	116	109	31	28	158	158	411	411
15	0	163	119	48	48	112	112	56	56
20	0	120	12	77	9	113	12	0	0
25	0	60	0	121	0	136	0	0	0
>25	0	250	0	834	0	261	0	0	0
min	0.75	0.59	0.59	0.09	0.09	0.09	0.09	0.09	0.09
max	5.88	68.17	15.71	89.27	15.44	39.42	15.79	13.07	13.07
average	3.26	21.76	9.23	38.94	8.42	14.78	5.98	4.74	4.74
std	2.97	15.12	3.85	20.24	4.67	10.95	4.05	2.88	2.88
Total rays out of 10,000	20	762	290	1150	124	1115	617	1113	1113
Total collection efficiency (8 element)	0.02		0.23		0.10		0.49		0.89

Fig. 3. Comparison of reflective optical elements.

during cellular respiration (Duysens and Amesz, 1957), to distinguish the presence of microbial contamination from environmental interferences. Measurement of the background in the off-cycle of a pulsed source allows contributions from other light sources to be subtracted from each measurement pulse. These devices employ specially designed low-noise analog circuits (Duncan and Powers, 2001), background cancellation techniques and algorithms (Wade et al., 2001), and approximate cancellation for the optical differences (e.g., scattering

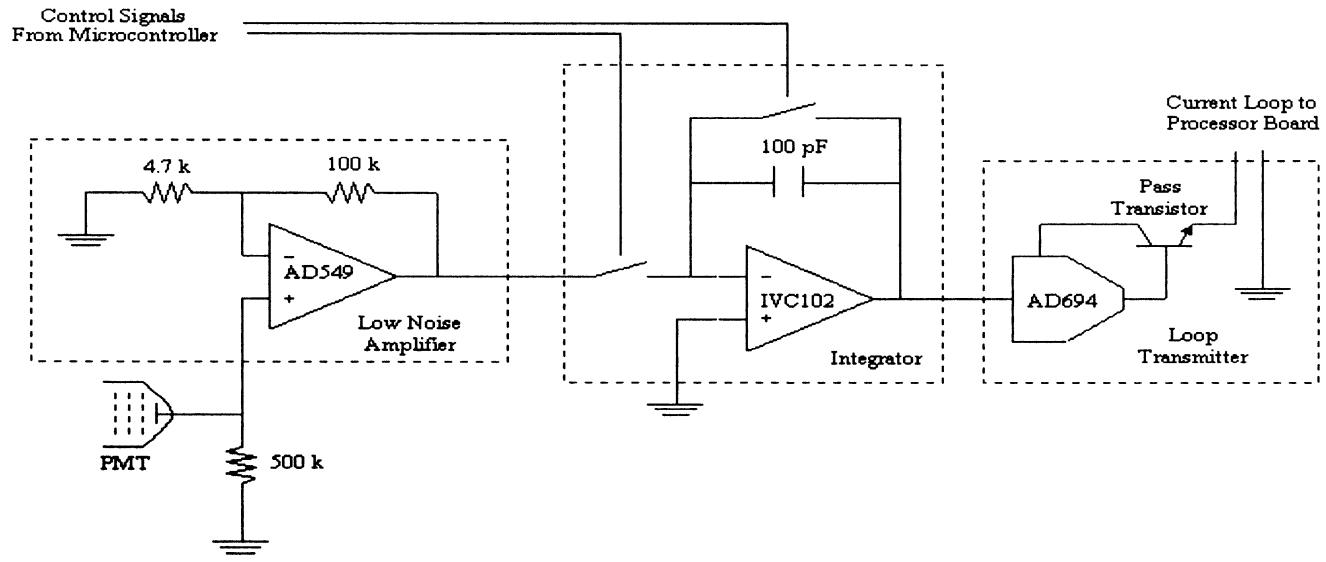

Fig. 4. Block diagram of the amplifier circuitry.

characteristics of the matrix, distance from the source of the fluorescence signals, penetration; Estes and Powers, 2001).

3.1. Optical design

In order to detect very low concentrations of microbes, the excitation light intensity must be maximized and all fluorescent photons not absorbed by the matrix must be collected and distinguished from the incident light. Conventional optical elements, like lenses and fiber optics, exhibit a low-level fluorescence in the blue region, which causes interference with the intrinsic fluorescence signals of the microbes. We have therefore used reflective optics to provide hemispherical collection of the fluorescence. Reflectors were designed and simulated using TracePro™ optical ray-tracing software provided by Lambda Research Corporation, Littleton, MA.

3.1.1. Excitation optics

In order to minimize the complexity of the overall mechanical design and to ensure continuity between measurements, it was decided to illuminate the surface of interest with all desired excitation wavelengths simultaneously. Band-pass interference filters are used for both excitation and emission. The interference filters have a band-pass width of 10 nm FWHM with 40% attenuation at the peak and an out-of-band pass attenuation of 10^6. Multiple filters increase the selectivity, but also attenuate the signal.

Band-pass interference filters require the incident light to be perpendicular to the filter surface. If the angle of incidence is $>15^\circ$, the band-pass shape deteriorates and the peak pass is shifted. In order for the simultaneous collection scheme to be effective, all lights must be collimated and perpendicular to the surface of the filter.

Broad-band illumination from a xenon flash lamp is collimated using a fused silica lens and passed to the excitation filters. Since each wavelength should illuminate the same spot on the sample, collimated light from each filter must be focused onto the sample (Fig. 2, middle). Polished metal mirrors are used to overlay and focus the three collimated excitation beams.

A two-surface focusing element is used to provide the focusing where each surface has a single curvature. After the excitation filter, each beam of excitation light hits a polished and chromed aluminum mirror, which has a curvature in the X-direction and flat in the Y-direction, and is mounted at 45° to the incident light. The light is passed to another mirror with a curvature in the Y-direction and flat in the X-direction at the appropriate angle so as to point the light on the desired spot on the sample (Fig. 2, right).

3.1.2. Emission optics

The sample emits fluorescence spherically and this fluorescence must be collimated for the interference filters and then focused on the photomultiplier tube (PMT) active surface. However, fluorescent photons are lost in reflection and it is important to minimize the number of reflections required to collect these photons. A reflective optical element collects the fluorescent light rays from the sample at the bottom and collimates it before passage through the filter and detection by the PMT. Using TracePro™ optical ray-tracing software, we find that the highest collection efficiencies at the PMT are produced by parabolic-type elements. Fig. 3 shows the results for several reflective elements including the numbers of reflections (bounces), angles of

incidence (minimum, maximum, average, and standard deviation), and collection efficiencies at the filters and PMTs corrected for the solid angle of collection. A paraboloid reflector allows ~90% of the rays emitted from the focal point to be collimated after reflection off the parabolic surface. By making the axial length of the reflector ~100 times larger than the focal length, the majority of the fluorescence photons "appear" to have come from the focal point. The sample is placed in the focal plane (Fig. 2, left). Mutiple separate paraboloids were arranged such that each shared the same focal point at the sample surface to collect different emission wavelengths. These were arranged to collect light from as much of the 180 sr emission as possible. At the end of each reflector are the band-pass filters followed by a focusing lens and photodetector (Fig. 2). The reflective collection elements using parabolas have been built and perform within our calculated errors.

3.2. Circuitry

The requirements for the amplifier circuitry are determined by three factors: the bandwidth of the light source, the output characteristics of the PMT, and the input characteristics of the A/D converters on board the microcontroller. To reduce coupling from high-frequency digital signals, the preamplifiers are built on a separate printed circuit board from the power supply and digital subsystems. In order to maximize the sensitivity of the instrument, noise and interference have been reduced to the minimum levels for the required gain and bandwidth. The primary sources of noise in a photocurrent preamplifier are thermal noise from the load resistor and shot noise from the PMT itself. The magnitudes of both noise sources are directly proportional to bandwidth. The design is comprised of three stages as shown in Fig. 4.

3.2.1. Gain stage

The pulsed xenon light source used for this design has an output rise time of approximately 10 μs and a half-maximum width of approximately 20 μs. Therefore, the amplifier will require a slew rate of 2 V/μs and a minimum bandwidth of 100 kHz. The first stage of the amplifier provides most of the gain. A typical PMT output current from a low concentration of cells is in the range 10–100 nA. Since the A/D converters use a 5 V scale reference, the amplifier must provide a minimum of 5×10^8 V/A gain. A load resistor can be used to provide a maximum gain of 3.0×10^5, as determined by the required bandwidth. An op-amp, configured as a non-inverting amplifier, is used as a buffer between the load resistor and the next stage of the circuit. To avoid loss of signal at the input, this op-amp must have a maximum input bias current of less than 10% of the smallest input signal over the entire operating temperature range. Several available low-input bias op-amps are suitable for this application. The AD549, manufactured by Analog Devices, meets the requirements with a minimum slew rate of 3 V/μs and a maximum input bias current of 250 fA. To reduce system noise, the bandwidth is chosen as the minimum possible for the given signal (with a small allowance for drift and tolerances).

To reduce offsets due to leakage currents, the inputs of the AD549 are surrounded by a guard trace. This trace is tied to the inverting input, which has a relatively low impedance path to ground. This diverts leakage currents to ground with a minimal offset voltage at the input.

3.2.2. Integrator

The second stage of the amplifier integrates the signal over the width of the lamp output pulse. This serves as an averaging function and acts as a sample-and-hold circuit to maintain the output during the A/D converter settling and acquisition time. The IVC102 single chip integrator, manufactured by Texas Instruments, provides a well-designed integrator in a single package. Integration and reset control are handled by a pair of logic-level control lines. The IVC102 serves as an excellent hold circuit due to its low (1 nV/μs) droop rate. The single chip design also allows for a compact circuit layout.

To reduce the effect of the electromagnetic pulse from the lamp, integration is started approximately 25 μs after the leading-edge of the lamp trigger signal. At this point, the signal pulse is near its peak magnitude and the electromagnetic interference from the lamp has decayed to nearly zero.

3.2.3. Output stage

The microcontroller selected for this design uses a single A/D converter multiplexed to eight input channels by a set of sample-and-hold circuits. This presents the output of the preamplifier with a low impedance. The input also exhibits a significant parallel capacitance. In order to minimize settling time, the output stage of the preamplifier is designed to have low output impedance and maximum stability for driving a capacitive load. This circuit uses an AD694 to convert the 0–10 V output of the integrator to a 0–16 mA current loop. Drift due to heat build-up is reduced by using an external pass transistor to source the output current. A load resistor converts this current to a voltage at the A/D converter input. Using a current loop to transmit the signal between printed circuit boards has the added benefit of lower susceptibility to electromagnetic interference. With the low output impedance of this design, the limiting factor for the settling time of the A/D input is the slew rate of the AD694.

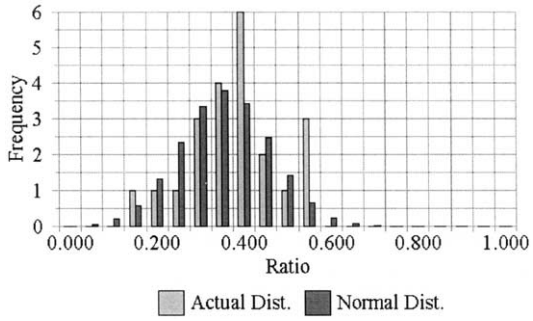

Fig. 5. Distribution of the fluorescence signal ratio distribution (440 nm/480 nm) for live bacterial cells.

3.3. Data analysis

The data from the PMTs must be normalized to a common gain and adjusted for variety of transmission properties of various interference filters.

3.3.1. Background compensation

The emitted light contains three main components: fluorescence from the intrinsic fluorophores, Rayleigh scattering, and stray light from the environment. The latter is measured in the off-cycle of the pulsed source and subtracted from the measured signal. Since only the fluorescence provides detection information, two methods have been used to compensate for the Rayleigh scattering components. The Rayleigh scattering is removed by finding two additional emission wavelengths at which essentially the entire signal is due to Rayleigh scattering. These two null emission points are used to fit a background curve using the Rayleigh scattering equation

$$I = \frac{a}{\lambda^4} + c,$$

where a is due to the intensity of the incident light, the number of scatterers, the polarization, the distance between the scatterers and the observer, and the angle between the incident light and the observer, and c is due to instrumentation. This curve then allows for the subtraction of Rayleigh scattering from the total emission signal, leaving only the desired fluorescence signals.

The ratio of the fluorescence signal to the scattered component of its excitation signal (measured directly or calculated as described above) approximately compensates for the differing properties of sample matrices and surfaces as well as the distance the measurement is made from the sample. Alternatively, ratios of the fluorescent signals can be used as the basis for detection. Furthermore, the relative amounts of these intrinsic fluorescence signals fall within well-defined physiological ranges (e.g., Fig. 5). Since, several fluorescence signatures are measured, whose ratios must fall within well-defined physiological limits, interference at any one of them can easily be detected and corrected. For example, pollen may exhibit tryptophan/tyrosine fluorescence, but certainly not other fluorescence signatures associated with metabolic intermediates or specific microbial proteins. Thus, the intensity of the tryptophan/tyrosine signature would be much too large compared with the intensities of the other signatures and would be discarded in the analysis. Fig. 6 shows a plot of pairs of ratios and the separation of the sample types (e.g., media and live bacterial cells).

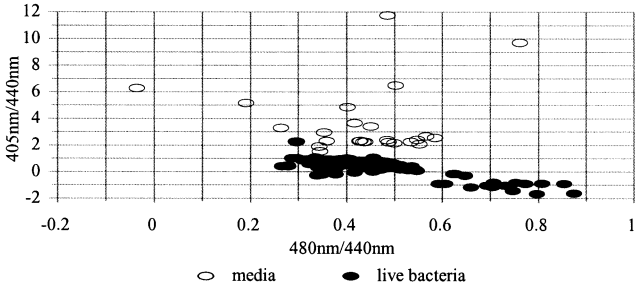

Fig. 6. Plot of the ratios of the intrinsic fluorescence emissions.

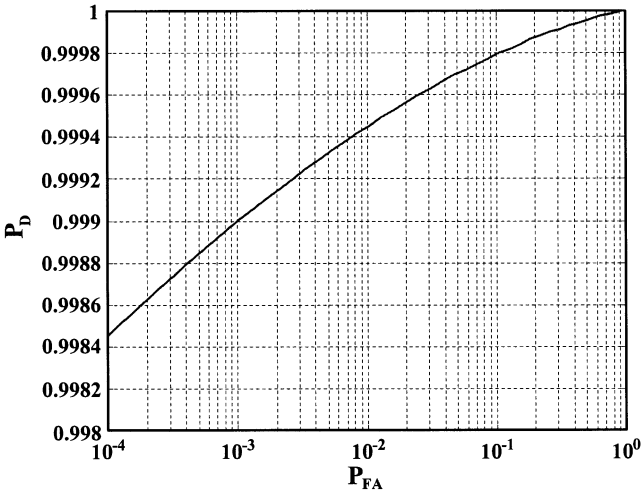

Fig. 7. Receiver operating curve for the Neyman–Pearson test.

3.3.2. Detection algorithm implementation

Three different algorithms were examined to determine their ability to distinguish samples containing bacteria, spores, and/or media (BSM) from those which do not.

3.3.2.1. Neyman–Pearson test. This test gives a probability of detection, pD, the probability that the test states that BSM are present when they indeed are, assuming a probability of false alarm, pFA, the probability that the test states that BSM are present when in fact they are not. This test requires knowledge of the ratio distributions for all types of samples likely to be encountered. A plot of the pFA versus pD gives the receiver-operating characteristic (ROC) which graphi-

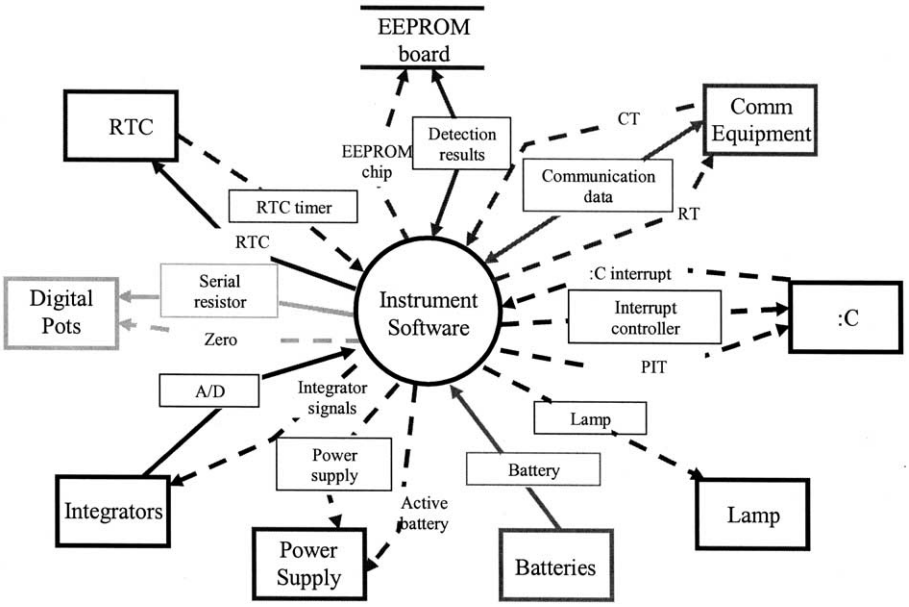

Fig. 8. Context level diagram for the control system.

cally presents the best choice for pFA and pD (Fig. 7). While the computations needed to produce the ROC for this case were extensive, applying the test only requires a few multiplication and comparison steps.

Given an assumed pFA of only 0.01%, the test indicates that the detection of bacteria, spores, and media would occur with a pD of more than 99% (Fig. 7). One drawback to the development of this algorithm is that it assumes that the distribution of the ratios is normal, which is not the case, and calculating the actual distributions would involve extensive computation.

3.3.2.2. Fuzzy logic. Fuzzy logic explicitly describes the degree to which an object belongs to a set by assigning it a fuzzy variable, a number between 0 and 1, inclusive, with numbers closer to 1 determining that an object belongs to the set with higher degree. In this application, fuzzy variables describe the degree to which a set of ratios from a sample belongs to the set of ratios described when no BSM are present versus those with bacteria present. Numbers above 0.5 identify the sample as containing BSM while those below 0.5 as not containing BSM. This algorithm successfully classified $\sim$91% of the samples with BSM correctly and 100% of the samples without BSM correctly, while it gives good detection results and takes less computing power than the Neyman–Pearson test.

3.3.2.3. Neural network. A neural network known as a multi-layer perceptron was used, which contains an input layer, an output layer, and one or more hidden layers, each with a given number of processing blocks known as neurons. The neurons for each layer are interconnected by weighted connections, which are linearly summed at each neuron and passed through a nonlinear function. The ratios are fed into the input layer, processed in the hidden layers, and then output to the output layer with a number between 0 and 1, with numbers above 0.5 identifying the sample as containing BSM and numbers below 0.5 as not containing BSM.

To function properly, the neural network must be first trained with data collected from samples that contain live bacteria, dead bacteria, spores, and media and also with samples that do not contain these (to obtain the weights for each connection). Different configurations of neural networks with 1–2 hidden layers and 1–7 neurons per hidden layer were trained using this data and tested with additional data of known composition. The neural network producing the greatest accuracy with the test data was chosen as the one used to implement the detection algorithm.

The neural network provided similar detection capabilities to the Neyman–Pearson test, but requiring only as much computation time as the fuzzy logic algorithm. Several neural network configurations successfully classified 100% of the BSM-containing samples and 100% of the non-BSM-containing samples. Furthermore, this algorithm could distinguish live cells, dead cells, spores, media, and water.

3.4. Controls

The microcontroller provides control for all the functions of the instrument. It takes data until a preset signal-to-noise ratio is achieved in the noisiest PMT, stores the data in on-chip memory and sends either raw or analyzed data via a wireless or satellite link to a user.

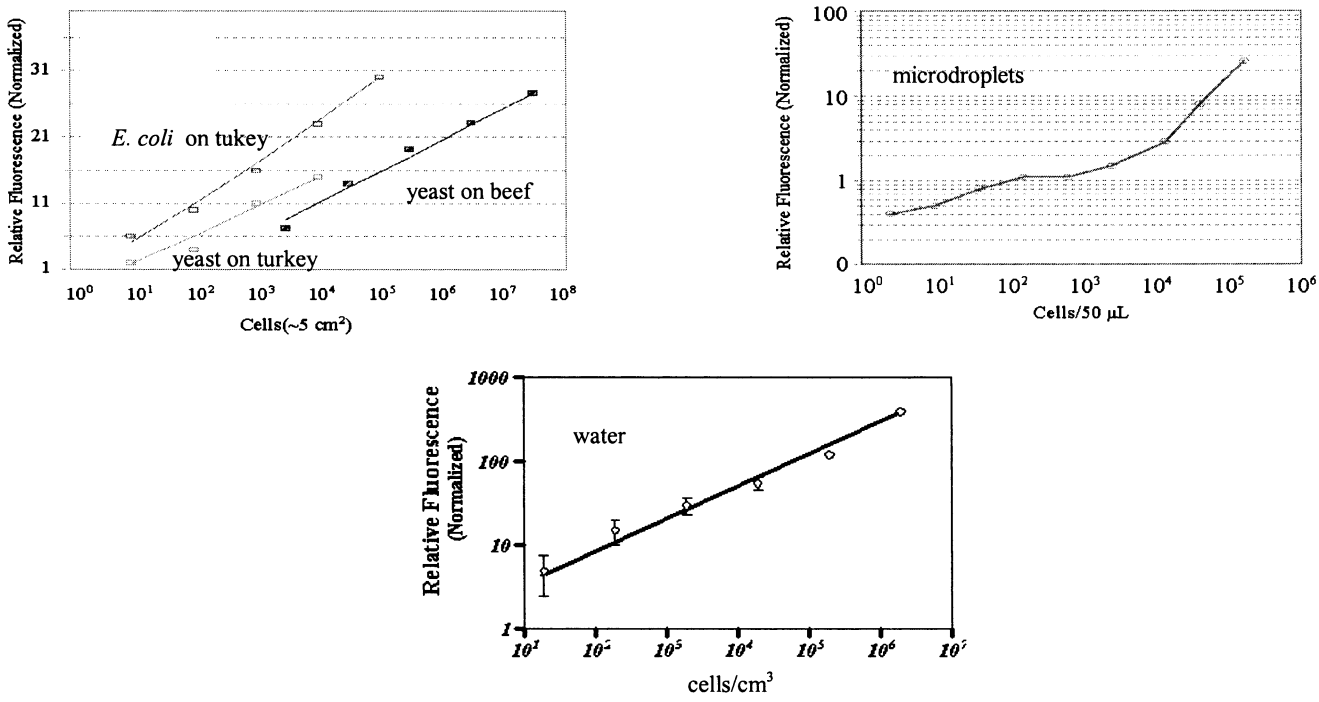

Fig. 9. Detection of microbial contamination on food (*Escherichia coli* and yeast) and in water (*E. coli*) using intrinsic RPN fluorescence.

It also performs self-test and calibration operations. Fig. 8 shows the context level diagram for the control system.

3.5. Data

The effect of various 'real-world' surfaces on measurements of microbial contamination have been investigated, including liquids, gases, foods, metals, ice, and a limited number of soil types. In many cases, 10–100 cells can be detected, regardless of the nature of the surface or the distribution of microbes. Examples of the RPN fluorescence of bacteria on food surfaces, in microdroplets (~ 50 µl) on surfaces, and in water are shown in Fig. 9.

4. Conclusions

These applications demonstrate the utility of a monitor for microbial contamination which is capable of distinguishing live cells, dead cells, spores, media, and water/air that requires no reagents, sample contact, and operates in near real-time (seconds). This system can be used as a trigger for an additional tier of identification analysis, such as PCR or immunological methods, as well as a reader for the capture of specific pathogens (emphasizing bacteria and viruses) or groups of related pathogens as described in the following paper.

Acknowledgements

This work was supported in part by DARPA under the Biosurveillance Program contract MDA972-97-1-12 and by the Willard L. Eccles Charitable Foundation.

References

Barlow, C., Chance, B., 1976. Ischemic areas in perfused rat hearts: measurement by NADH fluorescence photography. Science 193, 909–910.

Chance, B., Theorell, B., 1959. Localization and kinetics of reduced pyridine nucleotide in living cells by microfluorometry. J. Biol. Chem. 2234, 3044–3050.

Dalterio, R., Nelson, W., Britt, D., Sperry, J., Tanguay, J., Suib, S., 1987. The steady-state and decay characteristics of primary fluorescence from live bacteria. Appl. Spectrosc. 41, 234–241.

Duncan, A., Powers, L., 2001. Low noise amplification for optical arrays. In: Proceedings of the 23rd Annual International Conference of the IEEE Engineering in Medicine and Biology Society, Istanbul, Turkey, October 25–28, 2001.

Duysens, L., Amesz, J., 1957. Fluorescence spectrophotometry of reduced phosphopyridine nucleotide in intact cells in the near-ultraviolet and visible regions. Biochim. Biophys. Acta 24, 19–26.

Estes, C., Powers, L., 2001. Array-based design of multi-wavelength fluorescence system. In: Proceedings of the 23rd Annual International Conference of the IEEE Engineering in Medicine and Biology Society, Istanbul, Turkey, October 25–28, 2001.

Galeotti, T., van Rossum, G., Mayer, D., Chance, B., 1970. On the fluorescence of NAD(P)H in whole-cell preparations of tumors and normal tissues. Eur. J. Biochem. 17, 485–496.

Glazier, S., Weethall, H., 1994. Autofluorescence detection of *Escherichia coli* on silver membrane filters. J. Microbiol. Meth. 20, 23–27.

Henchal, E., Teska, J., Ludwig, G., Shoemaker, D., Ezzell, J., 2001. Current laboratory methods for biological threat agent identification. Clin. Lab. Med. 21 (3), 661–678.

Hobson, N., Tothill, I., Turner, A., 1996. Microbial detection. Biosens. Bioelectron. 11, 455–477.

Kierdaszuk, B., Malak, H., Gryczyski, I., Callis, P., Lakowicz, J., 1996. Fluorescence of reduced nicotinamides using one- and two-photon excitation. Biophys. Chem. 62, 1–13.

Lackowicz, J. (Ed.), 1991. Topics in Fluorescence Spectroscopy, Vol. 3, Plenum Press, New York.

Lloyd, C., Mason, H.-Y., Dice, M., Estes, C., Duncan, A., Wade, B., Ellis Jr., W., Powers, L., 2001. Microbioengineering: microbe capture and detection. In: Proceedings of the 23rd Annual International Conference of the IEEE Engineering in Medicine and Biology Society, Istanbul, Turkey, October 25–28, 2001.

Luong, J., Mulchandani, A., 1990. Applications of NADH-dependent fluorescence sensors for monitoring and controlling bioprocesses. Sens. Bioprocess Control 1, 75–94.

Mayevsky, A., Chance, B., 1982. Intracellular oxidation–reduction state measures in situ by a multichannel fiber optic surface fluorometer. Science 217, 537–540.

Nealson, K., Hastings, J., 1979. Bacterial bioluminescence: its control and ecological significance. Microbiol. Rev. 43, 496–518.

Powers, L., 1998. Method and apparatus for sensing the presence of microbes. US Patent 5,760,406.

Powers, L., 1999. Method and apparatus for sensing the presence of microbes. US Patent 5,968,766.

Powers, L., Ellis Jr., W., 2001. Taxonomic identification of pathogenic microorganisms and their toxic proteins. US Patent pending.

Powers, L., Lloyd, C., Ellis Jr., W., 2002. Method and apparatus for detecting the presence of microbes and determining their physiological status. US Patent pending.

Wade, B., Estes, C., Lloyd, C., Powers, L., 2001. Algorithm for recognition of optical spectra in an environment containing interferants. In: Proceedings of the 23rd Annual International Conference of the IEEE Engineering in Medicine and Biology Society, Istanbul, Turkey, October 25–28, 2001.